Inorg. Chem. **2004**, *43*, 7380–7388

Ultrafast Photochemical Dissociation of an Equatorial CO Ligand from *trans(X,X)*-[Ru(X)$_2$(CO)$_2$(bpy)] (X = Cl, Br, I): A Picosecond Time-Resolved Infrared Spectroscopic and DFT Computational Study

Anders Gabrielsson,[†] Stanislav Záliš,*[,‡] Pavel Matousek,[§] Mike Towrie,[§] and Antonín Vlček Jr.*[,†,‡]

Department of Chemistry and Centre for Materials Research, Queen Mary, University of London, Mile End Road, London E1 4NS, United Kingdom, J. Heyrovský Institute of Physical Chemistry, Academy of Sciences of the Czech Republic, Dolejškova 3, CZ-182 23 Prague, Czech Republic, and Central Laser Facility, CCLRC Rutherford Appleton Laboratory, Chilton, Didcot, Oxfordshire OX11 0QX, United Kingdom

Received April 6, 2004

Ultrafast photochemistry of the complexes *trans(X,X)*-[Ru(X)$_2$(CO)$_2$(bpy)] (X = Cl, Br, I) was studied in order to understand excited-state reactivity of equatorial CO ligands, coordinated *trans* to the 2,2′-bipyridine ligand (bpy). TD-DFT calculations have identified the lowest electronic transitions and singlet excited states as mixed X → bpy/Ru → bpy ligand to ligand/metal to ligand charge transfer (LLCT/MLCT). Picosecond time-resolved IR spectroscopy in the region of ν(CO) vibrations has revealed that, for X = Cl and Br, subpicosecond CO dissociation is accompanied by bending of the X–Ru–X moiety, producing a pentacoordinated intermediate *trans(X,X)*-[Ru(X)$_2$(CO)(bpy)]. Final movement of an axial halide ligand to the vacant equatorial position and solvent (CH$_3$CN) coordination follows with a time constant of 13–15 ps, forming the photoproduct *cis(X,X)*-[Ru(X)$_2$(CO)(CH$_3$CN)(bpy)]. For X = I, the opticaly populated ^{1}LLCT/MLCT excited state undergoes a simultaneous subpicosecond CO dissociation and relaxation to a triplet IRuI-localized excited state which involves population of an orbital that is σ-antibonding with respect to the axial I–Ru–I bonds. Vibrationally relaxed photoproduct *cis(I,I)*-[Ru(I)$_2$(CO)(CH$_3$CN)(bpy)] is formed with a time constant of ca. 55 ps. The triplet excited state is unreactive, decaying to the ground state with a 155 ps lifetime. The experimentally observed photochemical intermediates and excited states were assigned by comparing calculated (DFT) and experimental IR spectra. The different behavior of the chloro and bromo complexes from that of the iodo complex is caused by different characters of the lowest triplet excited states.

Introduction

Optical excitation of transition metal carbonyl complexes often results in breaking of a metal−CO bond. This is an ultrafast process, typically occurring on a femtosecond time scale. The structural variety of metal carbonyls that undergo photochemical CO dissociation is amazing. It includes simple homoleptic carbonyls such as Fe(CO)$_5$, M(CO)$_6$ (M = Cr, Mo, W), or Ni(CO)$_4$, as well as mixed-ligand complexes [M(CO)$_4$(diimine)], CpM(CO)$_2$ (M = Co, Rh, Ir), CpMn(CO)$_3$, and metal−carbonyl clusters and porphyrins.[1,2] The nature and dynamics of reactive excited states, excitation-energy dependence, the role of vibrational excitation, stereospecificity of the CO loss, competition with alternative relaxation and reaction pathways, and the factors limiting the photochemical quantum yield are of considerable fundamental and practical importance. Photodissociation of a CO ligand generates highly reactive coordinatively unsaturated species that can act in photocatalytic cycles or even activate C−H bonds in hydrocarbons.[3−6]

Mechanistically, a very interesting case is posed by carbonyl complexes containing electron-accepting ligands

* To whom correspondence should be addressed. E-mail: a.vlcek@qmul.ac.uk (A.V.); zalis@jh-inst.cas.cz (S.Z.).
[†] Queen Mary, University of London.
[‡] Academy of Sciences of the Czech Republic.
[§] CCLRC Rutherford Appleton Laboratory.

(1) Geoffroy, G. L.; Wrighton, M. S. *Organometallic Photochemistry*; Academic Press: New York, 1979.
(2) Roundhill, D. M. *Photochemistry and Photophysics of Metal Complexes*; Plenum Press: New York, 1994.
(3) Wrighton, M. S.; Ginley, D. S.; Schroeder, M. A.; Morse, D. L. *Pure Appl. Chem.* **1975**, *41*, 671−697.

10.1021/ic049548n CCC: $27.50
Published on Web 10/16/2004

such as $[M(CO)_4(\alpha\text{-diimine})]$ (M = Cr, Mo, W), $[Fe(CO)_3(\alpha\text{-diimine})]$, or $[Ni(CO)_2(\alpha\text{-diimine})]$; α-diimine = bipyridine, phenanthroline, diazabutadiene, 2-pyridylcarbaldehyde, and their derivatives.[7−25] The lowest excited state that is directly populated by optical excitation has a M → diimine metal to ligand charge transfer (MLCT) character. CO is an ancillary ligand which is not directly involved in MLCT excitation. Nevertheless, visible-light irradiation into the intense MLCT(diimine) transition triggers an ultrafast CO dissociation. This reaction was studied in detail for $[Cr(CO)_4(bpy)]$ and related $[M(CO)_4(\alpha\text{-diimine})]$ (M = Cr, Mo, W) complexes.[8−11,16−18,20,21] It was shown that CO dissociation in $[Cr(CO)_4(bpy)]$ occurs from a Franck−Condon ^{1}MLCT excited state within less than 400 fs after excitation.[9,10] The corresponding ^{3}MLCT(diimine) states are unreactive and decay to the ground state. The photochemical quantum yield is determined by branching of the Franck−Condon ^{1}MLCT excited-state evolution between CO dissociation and relaxation to the unreactive triplets.[9−11,20,26] Photochemical CO dissociation from $[M(CO)_4(diimine)]$ complexes is stereospecific, concerning only the axial CO ligand, that is coordinated perpendicularly to the M(diimine) plane.[9,11,12,14,15,17,18,20,21,23,27] Equatorial CO ligands in these complexes appear to be inert toward photodissociation.

Nevertheless, equatorial CO dissociation was observed[28−32] in the complexes *trans(X,X)*-$[Ru(X)_2(CO)_2(4,4'\text{-}R_2\text{-bpy})]$ (X = Cl, Br, I; R = H, C(O)OPr^i, C(O)OH, or Me). Irradiation into the lowest absorption band of the prototype complex *trans(Cl,Cl)*-$[Ru(Cl)_2(CO)_2(bpy)]$ in a CH_3CN or CH_3OH solution produces *cis(Cl,Cl)*-$[Ru(Cl)_2(CO)(solv)(bpy)]$.[28−30] Interestingly, CO substitution is accompanied by a shift of one halide ligand from the axial to the equatorial position.[29,30]

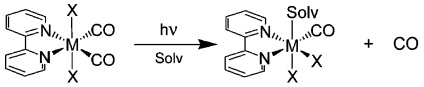

(1)

Equatorial CO loss is rather efficient, as is documented by the near-unity quantum yield values reported[28] for the photolysis of $[Ru(Cl)_2(CO)(bpy)]$ and values of 0.68 and 0.34 determined[31] for $[Ru(Br)_2(CO)_2(4,4'\text{-}(COOH)_2\text{-bpy})]$ and $[Ru(I)_2(CO)_2(4,4'\text{-}(COOH)_2\text{-bpy})]$, respectively. Prolonged irradiation of these complexes leads to a complete decarbonylation by substitution of the second CO ligand.[29,30]

Herein, we have chosen the complexes *trans(X,X)*-$[Ru(X)_2(CO)_2(bpy)]$ (X = Cl, Br, I) to investigate the mechanism and dynamics of photochemical dissociation of an equatorial CO from carbonyl−diimine complexes with a low-lying MLCT excited state. Moreover, the associated shift of an axial halide ligand poses further interesting mechanistic questions, namely whether it occurs simultaneously or subsequently to the dissociation of an equatorial CO ligand. These questions are addressed experimentally using picosecond time-resolved IR spectroscopy and theoretically, whereby DFT calculations are employed to reveal the nature of the low-lying excited states and to identify the experimentally observed intermediates.

Experimental Section

Materials. The complexes *trans(X,X)*-$[Ru(X)_2(CO)_2(bpy)]$ (X = Cl, Br, I) were synthesized according to the procedure described previously[29,30,33,34] and characterized by ^{1}NMR, ν(CO) IR, and UV−vis spectroscopy. All measurements were performed in CH_3CN (Aldrich spectroscopic grade).

Time-Resolved IR Spectroscopy, TRIR. Time-resolved IR measurements used the equipment and procedures described in detail previously.[35−39] In short, the sample solution was excited (pumped) at 400 nm, using frequency-doubled pulses from a Ti:sapphire laser of ∼150 fs duration (fwhm). TRIR spectra were

(4) Ford, P. C.; Boese, W.; Lee, B.; Macfarlane, K. L. In *Photosensitization and Photocatalysis Using Inorganic and Organometallic Compounds*; Kalyanasundaram, K., Grätzel, M., Eds.; Kluwer: Dordrecht, 1993; pp 359−390.
(5) Lees, A. J. *J. Organomet. Chem.* **1998**, *554*, 1−11.
(6) Bromberg, S. E.; Yang, H.; Asplund, M. C.; Lian, T.; McNamara, B. K.; Kotz, K. T.; Yeston, J. S.; Wilkens, M.; Frei, H.; Bergman, R. G.; Harris, C. B. *Science* **1997**, *278*, 260−263.
(7) Stufkens, D. J. *Coord. Chem. Rev.* **1990**, *104*, 39−112.
(8) Víchová, J.; Hartl, F.; Vlček, A., Jr. *J. Am. Chem. Soc.* **1992**, *114*, 10903−10910.
(9) Farrell, I. R.; Matousek, P.; Towrie, M.; Parker, A. W.; Grills, D. C.; George, M. W.; Vlček, A., Jr. *Inorg. Chem.* **2002**, *17*, 4318−4323.
(10) Farrell, I. R.; Matousek, P.; Vlček, A., Jr. *J. Am. Chem. Soc.* **1999**, *121*, 5296−5301.
(11) Vlček, A. J. *Coord. Chem. Rev.* **2002**, *230*, 225−242.
(12) Balk, R. W.; Snoeck, T.; Stufkens, D. J.; Oskam, A. *Inorg. Chem.* **1980**, *19*, 3015−3021.
(13) Wieland, S.; Reddy, K. B.; van Eldik, R. *Organometallics* **1990**, *9*, 1802−1806.
(14) Fu, W. F.; van Eldik, R. *Inorg. Chim. Acta* **1996**, *251*, 341−346.
(15) Fu, W.-F.; van Eldik, R. *Inorg. Chem.* **1998**, *37*, 1044−1050.
(16) Vlček, A., Jr.; Víchová, J.; Hartl, F. *Coord. Chem. Rev.* **1994**, *132*, 167−174.
(17) Virrels, I. G.; George, M. W.; Turner, J. J.; Peters, J.; Vlček, A., Jr. *Organometallics* **1996**, *15*, 4089−4092.
(18) Vlček, A., Jr. *Coord. Chem. Rev.* **1998**, *177*, 219−256.
(19) Vlček, A., Jr. *Coord. Chem. Rev.* **2000**, *200*−*202*, 933−977.
(20) Farrell, I. R.; Vlček, A., Jr. *Coord. Chem. Rev.* **2000**, *208*, 87−101.
(21) Guillaumont, D.; Daniel, C.; Vlček, A., Jr. *J. Phys. Chem. A* **2001**, *105*, 1107−1114.
(22) Guillaumont, D.; Daniel, C.; Vlček, A., Jr. *Inorg. Chem.* **1997**, *36*, 1684−1688.
(23) Grevels, F.-W.; Kerpen, K.; Klotzbücher, W.; Schaffner, K.; Goddard, R.; Weimann, B.; Kayran, C.; Özkar, S. *Organometallics* **2001**, *20*, 4775−4792.
(24) van Dijk, H. K.; Stufkens, D. J.; Oskam, A. *J. Am. Chem. Soc.* **1989**, *111*, 541−547.
(25) Servaas, P. C.; Stufkens, D. J.; Oskam, A. In *Photochemistry and Photophysics of Coordination Compounds*; Yersin, H., Vogler, A., Eds.; Springer-Verlag: Berlin, Heidelberg, 1987.
(26) Záliš, S.; Farrell, I. R.; Vlček, A., Jr. *J. Am. Chem. Soc.* **2003**, *125*, 4580−4592.
(27) Fu, W. F.; van Eldik, R. *Organometallics* **1997**, *16*, 572−578.
(28) Collomb-Dunand-Sauthier, M.-N.; Deronzier, A.; Ziessel, R. *J. Organomet. Chem.* **1993**, *444*, 191−198.
(29) Eskelinen, E.; Kinnunen, T.-J. J.; Haukka, M.; Pakkanen, T. A. *Eur. J. Inorg. Chem.* **2002**, 1169−1173.
(30) Eskelinen, E.; Haukka, M.; Venäläinen, T.; Pakkanen, T. A.; Wasberg, M.; Chardon-Noblat, S.; Deronzier, A. *Organometallics* **2000**, *19*, 163−169.
(31) Luukkanen, S.; Haukka, M.; Eskelinen, E.; Pakkanen, T. A.; Lehtovuori, V.; Kallioinen, J.; Myllyperkiö, P.; Korppi-Tommola, J. E. I. *Phys. Chem. Chem. Phys.* **2001**, *3*, 1992−1998.
(32) Lehtovuori, V.; Kallioinen, J.; Myllyperkiö, P.; Haukka, M.; Korpi-Tommola, J. *Chem. Phys.* **2003**, *295*, 81−88.
(33) Nieuwenhuis, H. A.; Stufkens, D. J.; Oskam, A. *Inorg. Chem.* **1994**, *33*, 3212−3217.
(34) Haukka, M.; Ahlgrén, M.; Pakkanen, T. A. *J. Chem. Soc., Dalton Trans.* **1996**, 1927−1933.
(35) Matousek, P.; Towrie, M.; Stanley, A.; Parker, A. W. *Appl. Spectrosc.* **1999**, *53*, 1485−1489.
(36) Matousek, P.; Towrie, M.; Ma, C.; Kwok, W. M.; Phillips, D.; Toner, W. T.; Parker, A. W. *J. Raman Spectrocopy* **2001**, *32*, 983−988.

probed with IR (~150 fs) pulses obtained by difference-frequency generation. The IR probe pulses cover a spectral range ca. 200 cm^{-1} wide. The pump and probe laser beams were focused to a spot of a maximum diameter of 200 μm. About 30 mL of sample solutions in CH_3CN flowed through a CaF_2 IR cell, which was rastered in two dimensions to minimize sample photolysis. Optical path lengths of 0.5−1 mm were used. The sample concentration was adjusted to achieve IR absorbance in the ν(CO) region of about 0.3. The spectra are reported at time delays of 2 ps and longer, when coherence effects fully subsided. All spectral and kinetic fitting procedures were performed using Microcal Origin 7 software.

Quantum Chemical Calculations. The ground-state electronic structures of all systems examined were calculated by density functional theory (DFT) methods using the Gaussian 03[40] and Turbomole[41] program packages. Low-lying excited states of the closed shell complexes were calculated by time-dependent DFT using the TD-DFT G03 program. Both Turbomole and Gaussian 03 were used for calculations of vibrational frequencies, which were performed at optimized geometries corresponding to the functional and basis set used. Excited-state IR spectra were modeled by unrestricted Kohn−Sham calculations for the lowest lying triplet states using the corresponding predominant single-determinant electron configurations.

The conductorlike screening model[42] (COSMO) incorporated within Turbomole was used for modeling of the solvent influence. The difference density plots were prepared using the GaussView software.

6-31G* polarized double-ζ basis sets[43] (geometry optimization) or correlation consistent polarized valence double ζ basis sets[44] (TD-DFT) were used for H, C, N, O, and Cl atoms, and the quasi-relativistic effective core pseudopotentials and the corresponding optimized set of basis functions were employed for I[45] and Ru.[46] In these calculations, either the hybrid Becke's three parameter functional with the Lee, Yang, and Parr correlation functional (B3LYP)[47] (G98/B3LYP) or the hybrid functional using Perdew, Burke, Ernzerhof[48] exchange and correlation functional with 25% HF exchange (PBE1PBE) was used.[49]

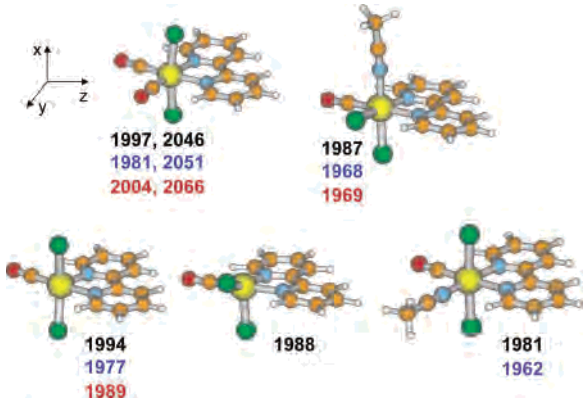

Figure 1. DFT-optimized structures of the *trans(Cl,Cl)*-$[Ru(Cl)_2(CO)_2$-(bpy)] (top left), its photoproduct *cis(Cl,Cl)*-$[Ru(Cl)_2(CO)(CH_3CN)$(bpy)] (top right), and possible photochemical intermediates (bottom row). ν(CO) IR wavenumbers are shown: G03/B3LYP/vacuum (black), Turbomole/B3LYP/COSMO in a CH_3CN solvent cage (blue), experimental values (red). The calculated ν(CO) values are scaled[51] by the factor 0.961.

Changes in electron-density distribution upon excitation were calculated as difference electron densities between the ground state and the investigated excited state, as described by TD-DFT (G03).

Geometry optimizations were carried out without any symmetry restrictions. The approximate C_{2v} symmetry was used for the description of the spectra and molecular orbitals. Here, the *z*-axis is coincident with the C_2 symmetry axis, the bpy ligand being located in the *yz*-plane, Figure 1.

Results

Calculation of Molecular Structures and ν(CO) IR Spectra. Molecular structures of *trans(Cl,Cl)*-$[Ru(Cl)_2(CO)_2$-(bpy)] and of several photochemical intermediates, optimized using G03/B3LYP−DFT calculations, are shown in Figure 1. The structure of *trans(I,I)*-$[Ru(I)_2(CO)_2$(bpy)] is very similar to that of the chloro complex. Selected calculated bond lengths and angles are summarized in the Supporting Information. The calculated structures well reproduce the experimental structures[31,50] of *trans(Cl,Cl)*-$[Ru(Cl)_2(CO)_2$-(bpy)] and *trans(I,I)*-$[Ru(I)_2(CO)_2$(4,4′-$(COOH)_2$-bpy)], namely the slight bending of the axial X−Ru−X moiety toward the bpy ligand.

Both complexes show a symmetrical (A_1) and antisymmetrical (B_1) ν(CO) vibrations at about 2000 and 2060 cm^{-1}, respectively. Ground-state ν(CO) wavenumbers of both complexes and of plausible photochemical intermediates were calculated using G03 or Turbomole software packages with the B3LYP functional. The calculated and experimental values are summarized in Figure 1. Generally, a reasonable agreement with experimental values for the starting complexes and their final photoproducts was obtained even using vacuum calculations. Calculations of the molecules in a CH_3-

(37) Towrie, M.; Grills, D. C.; Dyer, J.; Weinstein, J. A.; Matousek, P.; Barton, R.; Bailey, P. D.; Subramaniam, N.; Kwok, W. M.; Ma, C. S.; Phillips, D.; Parker, A. W.; George, M. W. *Appl. Spectrosc.* **2003**, *57*, 367−380.
(38) Vlček, A., Jr.; Farrell, I. R.; Liard, D. J.; Matousek, P.; Towrie, M.; Parker, A. W.; Grills, D. C.; George, M. W. *J. Chem. Soc., Dalton Trans.* **2002**, 701−712.
(39) Liard, D. J.; Busby, M.; Farrell, I. R.; Matousek, P.; Towrie, M.; Vlček, A., Jr. *J. Phys. Chem. A* **2004**, *108*, 556−567.
(40) Frisch, M. J.; Trucks, G. W.; Schlegel, H. B.; Scuseria, G. E.; Robb, M. A.; Cheeseman, J. R.; Montgomery, J. A., Jr.; Vreven, T.; Kudin, K. N.; Burant, J. C.; Millam, J. M.; Iyengar, S. S.; Tomasi, J.; Barone, V.; Mennucci, B.; Cossi, M.; Scalmani, G.; Rega, N.; Petersson, G. A.; Nakatsuji, H.; Hada, M.; Ehara, M.; Toyota, K.; Fukuda, R.; Hasegawa, J.; Ishida, M.; Nakajima, T.; Honda, Y.; Kitao, O.; Nakai, H.; Klene, M.; Li, X.; Knox, J. E.; Hratchian, H. P.; Cross, J. B.; Adamo, C.; Jaramillo, J.; Gomperts, R.; Stratmann, R. E.; Yazyev, O.; Austin, A. J.; Cammi, R.; Pomelli, C.; Ochterski, J. W.; Ayala, P. Y.; Morokuma, K.; Voth, G. A.; Salvador, P.; Dannenberg, J. J.; Zakrzewski, V. G.; Dapprich, S.; Daniels, A. D.; Strain, M. C.; Farkas, O.; Malick, D. K.; Rabuck, A. D.; Raghavachari, K.; Foresman, J. B.; Ortiz, J. V.; Cui, Q.; Baboul, A. G.; Clifford, S.; Cioslowski, J.; Stefanov, B. B.; Liu, G.; Liashenko, A.; Piskorz, P.; Komaromi, I.; Martin, R. L.; Fox, D. J.; Keith, T.; Al-Laham, M. A.; Peng, C. Y.; Nanayakkara, A.; Challacombe, M.; Gill, P. M. W.; Johnson, B.; Chen, W.; Wong, M. W.; Gonzalez, C.; Pople, J. A. *Gaussian 03*, revision B.01; Gaussian, Inc.: Pittsburgh, PA, 2003.
(41) Ahlrichs, R.; Bär, M.; Häser, M.; Horn, H.; Kölmel, C. *Chem. Phys. Lett.* **1989**, *162*, 165−169.
(42) Klamt, A.; Jones, V. *J. Chem. Phys.* **1996**, *105*, 9972.
(43) Hariharan, P. C.; Pople, J. A. *Theor. Chim. Acta* **1973**, *28*, 213.
(44) Woon, D. E.; Dunning, T. H., Jr. *J. Chem. Phys.* **1993**, *98*, 1358.
(45) Bergner, A.; Dolg, M.; Küchle, W.; Stoll, H.; Preuss, H. *Mol. Phys.* **1993**, *80*, 1431−1441.
(46) Andrae, D.; Häussermann, U.; Dolg, M.; Stoll, H.; Preuss, H. *Theor. Chim. Acta* **1990**, *77*, 123−141.
(47) Stephens, P. J.; Devlin, F. J.; Cabalowski, C. F.; Frisch, M. J. *J. Phys. Chem.* **1994**, *98*, 11623.
(48) Perdew, J. P.; Burke, K.; Ernzerhof, M. *Phys. Rev. Lett.* **1996**, *77*, 3865.
(49) Adamo, C.; Barone, V. *J. Chem. Phys.* **1999**, *110*, 6158.
(50) Haukka, M.; Kiviaho, J.; Ahlgrén, M.; Pakkanen, T. A. *Organometallics* **1995**, *14*, 825−833.

Table 1. DFT G03/B3LYP Calculated One-Electron Energies and Compositions of Selected Highest Occupied and Lowest Unoccupied Molecular Orbitals of *trans(Cl,Cl)*-[Ru(Cl)$_2$(CO)$_2$(bpy)] Expressed in Terms of Composing Fragments

MO	*E* (eV)	prevailing character	Ru	CO	Cl	bpy
			Unoccupied			
35a$_1$	−1.32	σ* Cl−Ru−Cl	26 (d$_{z^2}$); 29 (d$_{x^2-y^2}$)	11	28	6
8a$_2$	−1.98	π bpy		2		97
15b$_1$	−2.16	π bpy	1 (d$_{xz}$)			98
14b$_1$	−3.04	π bpy	1 (d$_{xz}$)	2	1	96
			Occupied			
7a$_2$	−6.05	Cl + Ru	34 (d$_{xy}$)	4	61	
13b$_1$	−6.12	Cl + Ru	30 (d$_{xz}$)	5	64	
34a$_1$	−6.97	Cl	5	1	92	2
26b$_2$	−6.98	Cl	5		92	3
12b$_1$	−7.61	Cl	6 (p$_x$)	2	85	7
6a$_2$	−7.69	π bpy	2 (d$_{xy}$)		2	96

Table 2. DFT G03/B3LYP Calculated One-Electron Energies and Compositions of Selected Highest Occupied and Lowest Unoccupied Molecular Orbitals of *trans(I,I)*-[Ru(I)$_2$(CO)$_2$(bpy)] Expressed in Terms of Composing Fragments

MO	*E* (eV)	prevailing character	Ru	CO	I	bpy
			Unoccupied			
7a$_2$	−1.87	π bpy		2		98
31a$_1$	−1.93	σ* I−Ru−I	3 (s); 18 (d$_{z^2}$); 27 (d$_{x^2-y^2}$)	6	43	2
11b$_1$	−2.09	π bpy		1		98
10b$_1$	−2.97	π bpy	1 (d$_{xz}$)	2	3	94
			Occupied			
6a$_2$	−5.78	I + Ru	18 (d$_{xy}$)		81	
9b$_1$	−5.81	I + Ru	15 (d$_{xz}$)	1	83	
30a$_1$	−6.24	I	4		95	
25b$_2$	−6.26	I	4		95	
8b$_1$	−6.83	I + Ru	9 (p$_x$); 4 (d$_{xz}$)	1	79	7
5a$_2$	−7.64	Ru	48 (d$_{xy}$)	9	13	30
7b$_1$	−7.80	Ru	60 (d$_{xz}$)	14	16	10
4a$_2$	−7.84	π bpy	13 (d$_{xy}$)	2	3	82

CN solvent cage increases the separation between the A_1 and B_1 vibrations, while shifting both ν(CO) wavenumbers below the experimental values.

Electronic Structure and Absorption Spectra. Tables 1 and 2 summarize Kohn−Sham frontier molecular orbitals of *trans(X,X)*-[Ru(X)$_2$(CO)$_2$(bpy)] X = Cl, I, calculated by G03/B3LYP. (Note that MO compositions depend little on the particular functional used.) Generally, the electronic structures of both complexes are characterized by a high degree of mixing between occupied Ru d$_\pi$ and X p$_\pi$ orbitals. The two highest occupied MOs are essentially X−Ru−X π-antibonding. The relative halide contribution increases on going from Cl to I, although the absolute calculated values may be somewhat exaggerated.[52] The occupied lower-lying 12b$_1$ and 8b$_1$ orbitals of the chloro and iodo complex, respectively, are weakly σ bonding with respect to the axial X−Ru−X moiety. The lowest unoccupied orbitals are bpy π*. They are followed in energy by an orbital that is σ-antibonding with respect to the X−Ru−X bond and partly Ru−CO π-antibonding. Notably, this σ* orbital lies at lower energy for X = I than Cl, 3.85 and 4.73 eV above the HOMO, respectively.

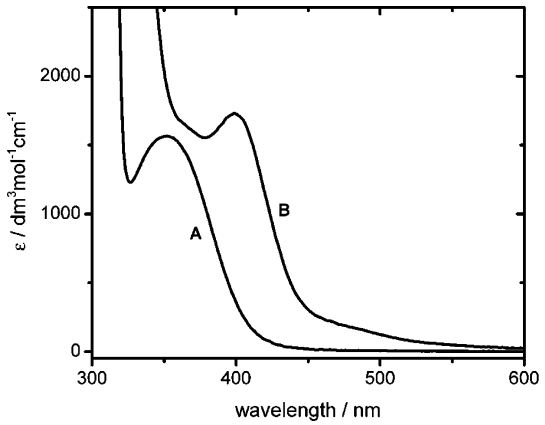

Figure 2. Electronic absorption spectra of *trans(Cl,Cl)*-[Ru(Cl)$_2$(CO)$_2$(bpy)] (A) and *trans(I,I)*-[Ru(I)$_2$(CO)$_2$(bpy)] (B) in CH_3CN.

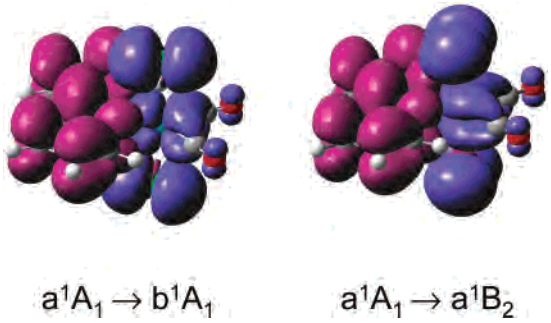

Figure 3. Changes of electron density distribution upon the two lowest electronic transitions of *trans(Cl,Cl)*-[Ru(Cl)$_2$(CO)$_2$(bpy)]. Blue and violet colors correspond to a decrease and increase of electron density, respectively.

Absorption spectra of both complexes are shown in Figure 2, and the calculated and experimental excitation energies are summarized in Tables 3 and 4.

The lowest absorption band of *trans(Cl,Cl)*-[Ru(Cl)$_2$(CO)$_2$(bpy)] at 352 nm ($\epsilon \cong 1560$ M^{-1} cm^{-1}) is attributed by TD-DFT predominantly to the a^{1}A$_1$ → b^{1}A$_1$ transition. Its mixed LLCT/MLCT character is obvious from the calculated changes of electron density distribution, see Figure 3, left. A weaker a^{1}A$_1$ → b^{1}B$_1$ LLCT transition lies at higher energy. The lowest in energy is the forbidden a^{1}A → a^{1}B$_2$ transition. It has a mixed LLCT/MLCT character, see Figure 3, right. As was found[52,53] for other halide complexes of low-valent metals, TD-DFT calculations underestimate energies of low-lying MLCT/LLCT transitions, although the characters of the transitions are well accounted for. The structured band between 270 and 320 nm corresponds to predominantly IL transitions.

trans(I,I)-[Ru(I)$_2$(CO)$_2$(bpy)] shows a broad absorption between 500 and 350 nm with an apparent maximum at 398 nm ($\epsilon \cong 1730$ M^{-1} cm^{-1}), Figure 2. The lowest allowed transition was identified as a^{1}A$_1$ → b^{1}A$_1$. It has the same LLCT/MLCT character as was discussed above for *trans-(Cl,Cl)*-[Ru(Cl)$_2$(CO)$_2$(bpy)], only with a higher LLCT contribution. Very close in energy lies the a^{1}A$_1$→b^{1}B$_1$ transition of a comparable intensity. It involves excitation into the 31a$_1$ σ* I−Ru−I orbital. It is very different from

(51) Wong, M. W. *Chem. Phys. Lett.* **1996**, *256*, 391−399.
(52) Turki, M.; Daniel, C.; Záliš, S.; Vlček, A., Jr.; van Slageren, J.; Stufkens, D. J. *J. Am. Chem. Soc.* **2001**, *123*, 11431−11440.
(53) Záliš, S.; Benamor, N.; Daniel, C. *Inorg. Chem.*, in press.

Table 3. Selected TD-DFT Calculated Excitation Energies of Lowest-Lying Singlet Electronic Transitions of *trans(Cl,Cl)*-[$Ru(Cl)_2(CO)_2(bpy)$] with Oscillator Strength Larger than 0.001

		G03/B3LYP		G03/PBE1PBE		experiment	
state	composition (G03/B3LYP)	transition, eV (nm)	osc str	transition, eV (nm)	osc str	expt	extinction coeff
b^1A_1	99% ($13b_1 \rightarrow 14b_1$)	2.37 (523)	0.006	2.56 (484)	0.007	3.52 (352)	1560
b^1B_1	86% ($13b_1 \rightarrow 35a_1$)	3.35 (370)	0.002	3.46 (358)	0.002		
d^1A_1	99% ($7a_2 \rightarrow 8a_2$)	3.38 (367)	0.005	3.63 (342)	0.005		
e^1A_1	97% ($12b_1 \rightarrow 14b_1$)	3.93 (315)	0.020	4.14 (299)	0.025		
d^1B_2	68% ($6a_2 \rightarrow 14b_1$); 17% ($5a_2 \rightarrow 14b_1$)	4.18 (297)	0.138	4.29 (289)	0.229		

Table 4. Selected TD-DFT Calculated Excitation Energies of Lowest-Lying Singlet Electronic Transitions of *trans(I,I)*-[$Ru(I)_2(CO)_2(bpy)$] with Oscillator Strength Larger than 0.001

		G03/B3LYP		G03/PBE1PBE		experiment	
state	composition (G03/B3LYP)	transition, eV (nm)	csc str	transition, eV (nm)	osc str	expt	extinction coeff
b^1A_1	99% ($9b_1 \rightarrow 10b_1$)	2.16 (574)	0.005	2.32 (534)	0.005	3.10−3.44 (398−360)	1730
b^1B_1	87% ($9b_1 \rightarrow 31a_1$); 5% ($7b_1 \rightarrow 31a_1$)	2.78 (446)	0.004	2.85 (435)	0.004		
d^1A_1	67% ($6a_2 \rightarrow 7a_2$); 28% ($8b_1 \rightarrow 10b_1$)	3.24 (383)	0.005	3.27 (379)	0.018		
e^1A_1	63% ($8b_1 \rightarrow 10b_1$); 32% ($6a_2 \rightarrow 7a_2$)	3.29 (377)	0.038	3.48 (356)	0.024		
e^1B_1	55% ($7b_1 \rightarrow 31a_1$); 26% ($8b_1 \rightarrow 31a_1$)			4.39 (282)	0.090		
e^1B_2	50% ($4a_2 \rightarrow 10b_1$); 30% ($8b_1 \rightarrow 7a_2$)			4.41 (281)	0.090		

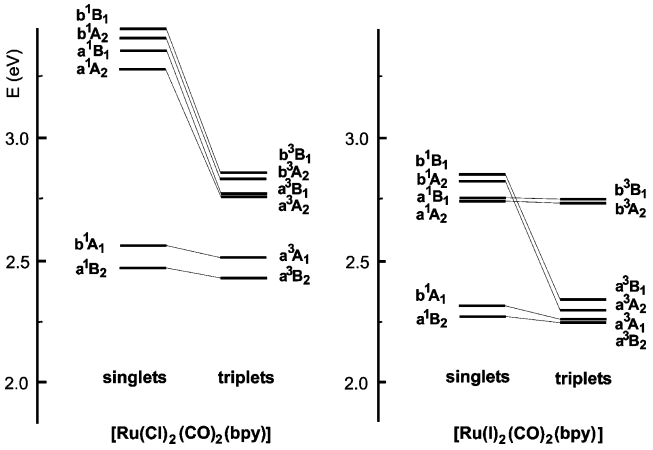

Figure 4. Correlation diagram of the TD-DFT (G03/PBE1PBE) calculated low-lying singlet and triplet excited states of *trans(Cl,Cl)*-[$Ru(Cl)_2(CO)_2$(bpy)] and *trans(I,I)*-[$Ru(I)_2(CO)_2$(bpy)] complexes.

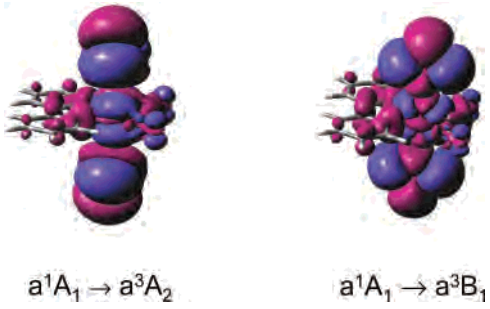

Figure 5. Changes of electron density distribution upon the $a^1A_1 \rightarrow a^3A_2$ and $a^1A_1 \rightarrow a^3B_1$ triplet electronic transitions of *trans(I,I)*-[$Ru(I)_2(CO)_2$(bpy)]. Changes of electron density upon the corresponding singlet transitions are virtually identical. Blue and violet colors correspond to a decrease and increase of electron density, respectively.

the corresponding transition of the chloro complex. Qualitatively, the $a^1A_1 \rightarrow b^1B_1$ transition of *trans(I,I)*-[$Ru(I)_2(CO)_2$(bpy)] involves transfer of electron density from d_π to d_σ orbitals of the I−Ru−I bonds and a massive reorientation of electron density at the halide atoms, Figure 5. Hereinafter, it will be known as an IRuI-localized transition. The relative energies of the $a^1A_1 \rightarrow b^1A_1$ and $a^1A_1 \rightarrow a^1B_1$ transitions depend somewhat on the functional used. The actual energy order of these two transitions could depend on the medium, since larger solvatochromism is expected for the MLCT/LLCT $a^1A_1 \rightarrow b^1A_1$ transition than for the IRuI-localized $a^1A_1 \rightarrow a^1B_1$. The next higher-lying transition is $a^1A_1 \rightarrow d^1A_1$, which can also contribute to the lowest absorption band. It has an LLCT character with a minor $\sigma\pi^*$, that is, σ bond to ligand charge transfer, contribution.

Table 5. TD-DFT Calculated Low-Lying Triplet Excitation Energies of *trans(I,I)*-[$Ru(I)_2(CO)_2$(bpy)]

state	character	G03/B3LYP transition, eV (nm)	G03/PBE1PBE, transition, eV (nm)
a^3B_2	99% ($6a_2 \rightarrow 10b_1$)	2.08	2.23
a^3A_1	99% ($9b_1 \rightarrow 10b_1$)	2.10	2.25
a^3A_2	87% ($6a_2 \rightarrow 31a_1$)	2.29	2.30
a^3B_1	83% ($9b_1 \rightarrow 31a_1$); 12% ($30a_1 \rightarrow 10b_1$)	2.35	2.36

Shown in Figure 4 are correlation diagrams between triplet and singlet states of the two complexes. *trans(Cl,Cl)*-[$Ru(Cl)_2(CO)_2$(bpy)] has a^3B_2 and a^3A_1 lowest-lying triplet states. They have the same LLCT/MLCT character as the corresponding singlets, see Figure 3. The next higher state is a^3A_2, which involves population of the σ^* orbital. It lies 0.47 eV above the a^3A_1 state. The situation is profoundly different for *trans(I,I)*-[$Ru(I)_2(CO)_2$(bpy)], see Figure 4 and Table 5. A manifold of very closely spaced four triplet states is present. Two of them, a^3B_2 and a^3A_1, have the usual LLCT/MLCT character, whereas the a^3A_2 and a^3B_1 states involve excitation into the σ^*(I−Ru−I) orbital, acquiring a IRuI-localized character. The changes in electron density distribution upon population of the a^3A_2 and a^3B_1 states are shown in Figure 5. The TD-DFT calculated energies of the four lowest triplet states are very close to each other. In contrast to TD-DFT, single-determinant Kohn−Sham geometry optimization yields a^3A_2 as the lowest state. DFT calculations alone thus cannot unequivocally predict which triplet state of *trans(I,I)*-[$Ru(I)_2(CO)_2$(bpy)] will be the lowest at the relaxed geometry and solvent environment. Comparison between calculated and experimental excited-state IR spectra indicates the IRuI-localized a^3A_2 state to be the lowest triplet state, vide infra.

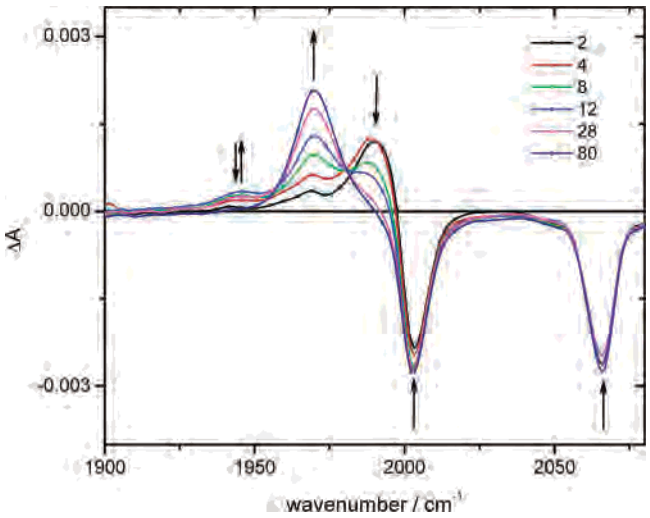

Figure 6. Difference time-resolved IR spectra of *trans(Cl,Cl)*-[$Ru(Cl)_2(CO)_2(bpy)$] measured in CH_3CN at 2, 4, 8, 12, 28, and 80 ps after ~150 fs, 400 nm laser pulse excitation. The spectra evolve in the direction of the arrows. Experimental points are separated by 4−5 cm^{-1}.

Time-Resolved IR Spectroscopy (TRIR). *trans(Cl,Cl)*-[$Ru(Cl)_2(CO)_2(bpy)$] and *trans(Br,Br)*-[$Ru(Br)_2(CO)_2$-(bpy)]. TRIR spectra (Figure 6) of [$Ru(Cl)_2(CO)_2(bpy)$] consist of four spectral features: (i) two negative bands (bleaches) due to depleted ground-state absorption at 2004 and 2066 cm^{-1}; (ii) a transient band at 1989 cm^{-1} that is attributed to a pentacoordinated intermediate *trans(Cl,Cl)*-[$Ru(Cl)_2(CO)(bpy)$], see below; (iii) a band at 1969 cm^{-1} that is assigned to the *cis(Cl,Cl)*-[$Ru(Cl)_2(CO)(CH_3CN)(bpy)$] photoproduct by comparison with the IR spectrum of an authentic, crystallographically characterized[30] sample; (iv) a very weak shoulder at 1941−1945 cm^{-1} that belongs either to an unidentified side-product or to a vibrationally excited species.

The assignment of the 1989 cm^{-1} transient band to *trans(Cl,Cl)*-[$Ru(Cl)_2(CO)(bpy)$] is based on DFT calculations. The spectral pattern consisting of a single ν(CO) band shows that the intermediate is a monocarbonyl species. In principle, we can consider a trigonal bipyramidal or square pyramidal structures with *trans(Cl,Cl)* or *cis(Cl,Cl)* geometries. To identify the most probable intermediate structure, we have calculated ν(CO) wavenumbers of the parent complex, the photoproduct *cis(Cl,Cl)*-[$Ru(Cl)_2(CO)(CH_3CN)(bpy)$], and several possible intermediates, see Figure 1. To agree with the trend in the experimental TRIR spectra, the calculated intermediate ν(CO) wavenumber has to be higher than the value calculated for the photoproduct. Calculations with different initial geometries of the intermediate produced two different optimized geometries, that correspond to two local minima on the potential energy surface. They essentially differ only in the Cl−Ru−Cl bonding angle. One intermediate approaches a trigonal bipyramidal *cis(Cl,Cl)*-[$Ru(Cl)_2$-(CO)(bpy)] structure, with the Cl−Ru−Cl angle of 116.7°. Its ν(CO) wavenumber calculated in a vacuum is essentially identical with that calculated for the photoproduct. A solution value could not have been obtained since the calculation did not converge. The second intermediate structure can be approximately described as *trans(Cl,Cl)*-[$Ru(Cl)_2(CO)(bpy)$] with vacancy in the equatorial plane. The calculated ν(CO) wavenumber is 7 cm^{-1} (G03, vacuum) or 9 cm^{-1} (Turbomole, CH_3CN) higher than the calculated photoproduct wavenumber, see Figure 1, bottom left. Although the calculated difference in ν(CO) wavenumbers of the intermediate and photoproduct is smaller than the experimental value of 20 cm^{-1}, the direction of the change is correct, and this result is a good indication for *trans(Cl,Cl)*-[$Ru(Cl)_2(CO)$-(bpy)] being the primary intermediate. The DFT optimized geometry shows that the Cl−Ru−Cl moiety is bent (162.7°) toward the vacant position. Considering that the Cl−Ru−Cl moiety in the parent complex is bent toward the bpy ligand by 9.5°, it follows that the CO dissociation is accompanied by bending of the Cl−Ru−Cl moiety by 26.8°. We have also investigated the effect of solvent coordination on the intermediate structure. The ν(CO) wavenumber for *trans-(Cl,Cl)*-[$Ru(Cl)_2(CO)(CH_3CN)(bpy)$] was calculated lower than for the photoproduct both in a vacuum and the solvent cage, indicating that it cannot correspond to the observed intermediate.

The temporal evolution of TRIR spectra of *trans(Cl,Cl)*-[$Ru(Cl)_2(CO)_2(bpy)$] shows (Figure 6) that both bleach bands and the 1989 cm^{-1} intermediate band (which partly overlaps with the 2004 cm^{-1} bleach) are formed "instantaneously" within the instrument time resolution. These features are well developed already in the spectrum measured at 2 ps after 400 nm excitation. The intensity of the 1989 cm^{-1} intermediate band rapidly decays with a time constant of 10.0 ± 1.6 ps while the 1969 cm^{-1} product band grows in with a similar time constant of 13.7 ± 1.0 ps. The presence of an isosbestic point and similar time constant values testify to a direct conversion of the *trans(Cl,Cl)*-[$Ru(Cl)_2(CO)(bpy)$] intermediate into the *cis(Cl,Cl)*-[$Ru(Cl)_2(CO)(CH_3CN)(bpy)$] product. The apparently faster decay of the 1989 cm^{-1} band is most probably caused by interfering 5.0−6.5 ps band narrowing. This is manifested by an early deepening of the overlapping 2004 cm^{-1} bleach, probed at 1997 cm^{-1}. The intensity of the higher bleach band at 2066 cm^{-1} is time-independent in the 2−1000 ps time range investigated, excluding the presence of any recombination with free CO. The weak shoulder between 1941 and 1945 cm^{-1} grows during the first 10 ps and then decays to a constant background in the next ca. 50 ps.

TRIR spectra of *trans(Br,Br)*-[$Ru(Br)_2(CO)_2(bpy)$] show essentially the same behavior as that described above for the chloro complex. The intermediate band at 1983 cm^{-1} decays with a time constant of 14 ± 3 ps, being converted to a photoproduct whose peak at 1969 cm^{-1} grows with an identical time constant of 15 ± 1 ps. In addition, a very weak shoulder appears transiently at ca. 1941 cm^{-1}. This feature grows within the first 5−6 ps and disappears at 100 ps.

***trans(I,I)*-[$Ru(I)_2(CO)_2(bpy)$].** TRIR spectra (Figure 7) show that excitation of *trans(I,I)*-[$Ru(I)_2(CO)_2(bpy)$] in CH_3-CN ultimately leads to a monocarbonyl product *cis(I,I)*-[$Ru(I)_2(CO)(CH_3CN)(bpy)$], that is characterized[31] by a ν(CO) band at 1967 cm^{-1}. However, the excited-state behavior of *trans(I,I)*-[$Ru(I)_2(CO)_2(bpy)$] is very different from those of the chloro and bromo complexes. The TRIR spectra of *trans-*

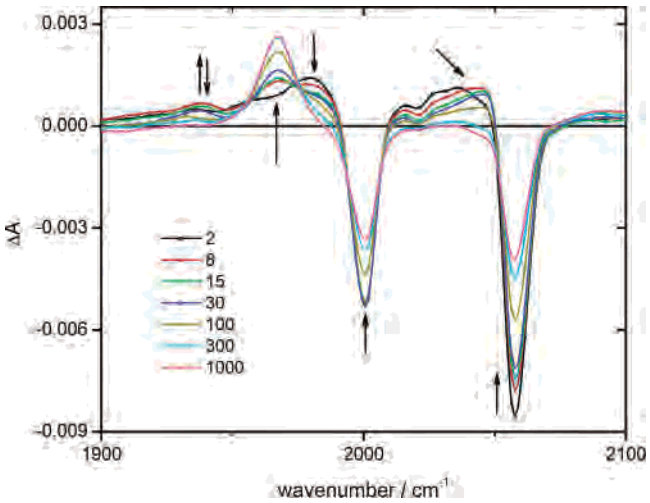

Figure 7. Difference time-resolved IR spectra of *trans(I,I)*-[$Ru(I)_2(CO)_2$-(bpy)] measured in CH_3CN at 2, 8, 15, 30, 100, 300, and 1000 ps after ~150 fs, 400 nm laser pulse excitation. The spectra evolve in the direction of the arrows. Experimental points are separated by 4−5 cm^{-1}.

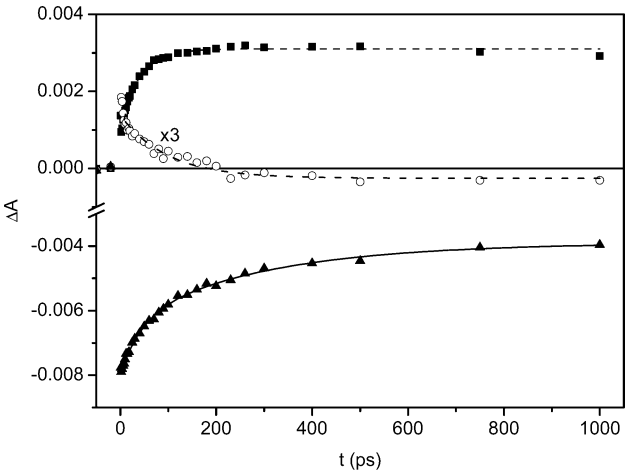

Figure 8. Photodynamics of *trans(I,I)*-[$Ru(I)_2(CO)_2$(bpy)] in CH_3CN. Kinetic profiles of the absorbance due to the photoproduct at 1967 cm^{-1} (top, ■), the IRuI-localized $^3A_2$ excited state at 2036 cm^{-1} (top, ○, values multiplied by the factor of 3), and the ground-state bleach at 2059 cm^{-1} (bottom, ▲). The growth of the product is faster (55 ± 15 ps) than the $^3A_2$ excited-state decay and the bleach recovery, which occur with a common time constant of ca. 155 ps. (The absorbance at 2036 cm^{-1} is slightly negative at long time delays because of an overlap with the bleach ground-state absorption.)

(I,I)-[$Ru(I)_2(CO)_2$(bpy)] exhibit the following four features: (i) bleached ground-state bands at 2000 and 2059 cm^{-1}; (ii) a photoproduct band at 1967 cm^{-1} that grows in; (iii) two transient bands at ca. 1981 and 2045 cm^{-1} whose long-time decay kinetics are similar within the experimental accuracy. This feature belongs to a dicarbonyl species whose ν(CO) bands are downshifted from the ground-state values. It was assigned by DFT to the IRuI-localized $^3A_2$ excited state: DFT(G03) vacuum calculation yields the ν(CO) vibrations of *trans(I,I)*-[$Ru(I)_2(CO)_2$(bpy)] at 1997 and 2041 cm^{-1} in the ground state and at 1966, 2017 cm^{-1} in the $^3A_2$ excited state. The calculated downward shift is in a reasonable agreement with the experimental observation, given that the wavenumbers are calculated in a vacuum and that the 1981 cm^{-1} band is broadened on its low-wavenumber side indicating that the actual excited-state ν(CO) wavenumber could be somewhat lower. Initially, the 1981 cm^{-1} is more intense than the 2030−2045 cm^{-1} but these two IR features become comparable in intensity after about 10 ps. It appears that the 1981 cm^{-1} initially contains a second component, which is also responsible for its extensive broadening on the low-energy side. By analogy with the chloro complex, it is attributed to the pentacoordinated *trans(I,I)*-[$Ru(I)_2(CO)$-(bpy)] intermediate. (iv) Also, there is a weak feature at 1935 cm^{-1} that is due to an unidentified side-product or a vibrationally excited species.

Strong overlap between the transient IR features and the bleached ground-state bands and the early vibrational dynamics, which are manifested by band narrowing and shifts, complicates detailed kinetic analysis of the data. Nevertheless, it is possible to distinguish four distinct time domains: (i) First we describe features formed within the instrument time resolution. TRIR spectra measured immediately (1−2 ps) after excitation show bleached ground-state bands at 2000 and 2059 cm^{-1}, a broad $^3A_2$ excited-state absorption between 2030 and 2045 cm^{-1} and at 1981 cm^{-1}, and a very weak feature at ca. 1935 cm^{-1}. The 1981 cm^{-1} band is intense and strongly broadened at its low-wavenumber side, apparently due to an overlap between the excited-state and hot photointermediate absorptions, vide supra.

(ii) There are also the early spectral changes (2−20 ps). The 2030−2045 cm^{-1} band narrows and its maximum shifts to its final position of ~2045 cm^{-1} during the first 20 ps. This is manifested by decay at 2030−2035 cm^{-1} and a small initial rise at 2045−2050 cm^{-1}. The 1981 cm^{-1} band undergoes a rapid partial decay during the first 10−15 ps.

(iii) The 20−100 ps range. The photoproduct feature at 1967 cm^{-1} grows in from a broad background with a time constant of 55 ± 15 ps, see Figure 8, top. The weak 1935 cm^{-1} feature slightly increases in intensity during the first ~10 ps and then decays. Biexponential fitting yielded a 9 ± 2 and 51 ± 6 ps rise and decay time constants. respectively.

(iv) Also, there are later spectral changes, >100 ps. The product band stays constant at longer time scale while the $^3A_2$ excited-state features (2045, 1981 cm^{-1}) decay and the bleach bands recover with a common time constant of ca. 155 ps, see Figure 8. No spectral changes occur on a time scale longer than ca. 600 ps.

Discussion

Electronic structures of the complexes *trans(X,X)*-[$Ru(X)_2$-$(CO)_2$(bpy)] (X = Cl, I) are characterized by highest occupied orbitals with strongly mixed $Ru(d_\pi)/X(p_\pi)$ character. The lowest unoccupied MOs are almost entirely bpy(π^*). Interestingly, an unoccupied Ru−X σ-antibonding orbital occurs at relatively low energies. It originates in an out-of-phase overlap between the symmetric combination of halide p_σ orbitals with $Ru(d_\sigma)$ orbitals. Population of this σ^* MO upon electronic excitation has profound photochemical consequences, as will be discussed below.

Scheme 1. Proposed Mechanism of Photochemical CO Substitution/Isomerization of *trans(Cl,Cl)*-[$Ru(Cl)_2(CO)_2(bpy)$]

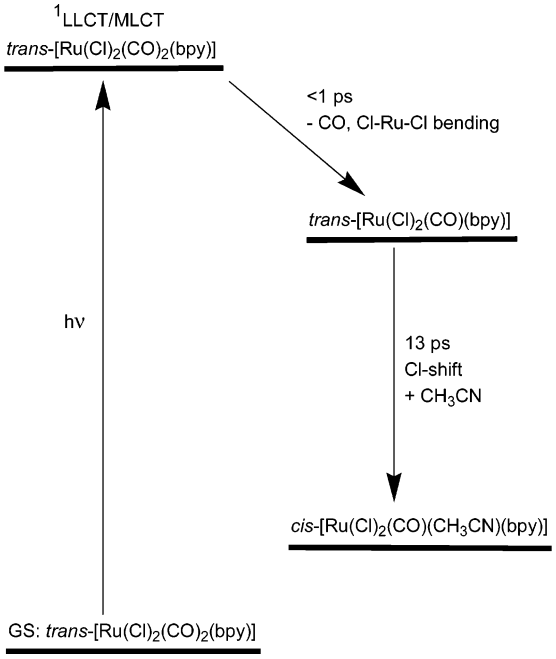

Scheme 2. Proposed Mechanism of Photochemical CO Substitution/Isomerization of *trans(I,I)*-[$Ru(I)_2(CO)_2(bpy)$]

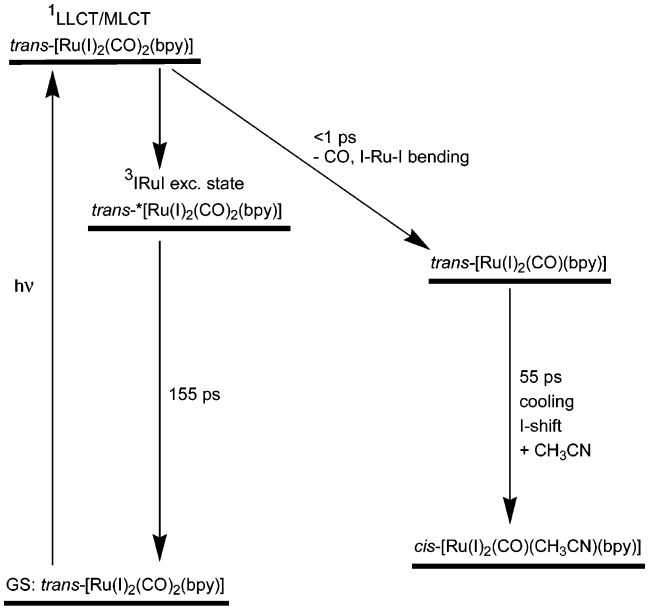

TD-DFT analysis and assignment of electronic transitions show that 400 nm laser pulse irradiation of *trans(X,X)*-[$Ru(X)_2(CO)_2(bpy)$] (X = Cl, Br, I) excites predominantly the $a^1A_1 \rightarrow b^1A_1$ LLCT/MLCT electronic transition. Previous studies have shown that the same overall photochemical reaction (eq 1) occurs for X = Cl, Br, and I, although the quantum yield drops in the order Cl > Br > I.[28,31] An equatorial CO ligand is lost upon excitation, and its position is occupied by one of the halide ligands that shifts from the axial position, eq 1. Nevertheless, the results presented above demonstrate that the excited-state dynamics and photochemical mechanisms are profoundly different for the chloro and bromo complexes on one side and the iodo complex on the other.

For *trans(Cl,Cl)*-[$Ru(Cl)_2(CO)(bpy)$] (Scheme 1), excitation into the lowest absorption band triggers an ultrafast (<1 ps) dissociation of a Ru−CO bond that yields a pentacoordinated *trans(Cl,Cl)*-[$Ru(Cl)_2(CO)(bpy)$] intermediate with a coordination vacancy in the equatorial Ru(bpy) plane, *trans* to the bpy ligand, Figure 1, bottom left. DFT calculations indicate that the CO dissociation is accompanied by symmetrical bending of the Cl−Ru−Cl unit by about 27°. It can be concluded that the first stage of the Cl-ligand movement is concerted with the Ru−CO bond breaking. The second reaction step follows with a rate constant of 13 ps. It involves the final movement of a Cl ligand to the vacant equatorial position, accompanied by coordination of a CH_3CN solvent molecule at the axial position. The final product, *cis(Cl,Cl)*-[$Ru(Cl)_2(CO)(CH_3CN)(bpy)$], is formed. The same mechanism operates for *trans(Br,Br)*-[$Ru(Br)_2(CO)_2(bpy)$], for which the second step occurs with a time constant of ca. 15 ps.

TRIR experiments show no signs of any LLCT/MLCT excited state of the parent molecule *trans(Cl,Cl)*-[$Ru(Cl)_2(CO)_2(bpy)$], whose population would precede the CO loss. Unreactive "trapping" spin-triplet LLCT/MLCT states were not observed either.[54] This, together with the femtosecond rate of CO dissociation, implies that potential energy surfaces of the optically excited b^1A_1 and/or the lower-lower lying a^1B_2 singlet states are dissociative. The Ru−CO dissociation is much faster than relaxation (intersystem crossing) to any ^{3}LLCT/MLCT state or internal conversion to the ground state. This conclusion agrees with the near-unity quantum yield[28] of the photochemical CO substitution in *trans(Cl,Cl)*-[$Ru(Cl)_2(CO)_2(bpy)$].

The LLCT/MLCT character of the b^1A_1 and a^1B_2 (Figure 3) itself does not warrant a dissociative character. Its potential energy surface most probably becomes dissociative through a strongly avoided crossing with higher-lying LF-type state(s) along the reaction coordinate, resulting in an ultrafast CO dissociation. The same behavior is exhibited by ^{1}MLCT excited states of [$Cr(CO)_4(bpy)$] and other metal carbonyls.[16,18,21,55−59]

For *trans(I,I)*-[$Ru(I)_2(CO)(bpy)$], the optically populated ^{1}LLCT/MLCT excited state undergoes parallel subpicosecond CO dissociation coupled with I−Ru−I bending and an intersystem crossing to triplet IRuI-localized excited $^3A_2$ and, possibly, also the $^3B_1$ state, see Scheme 2. The *trans(I,I)*-[$Ru(I)_2(CO)(bpy)$] intermediate appears to be initially formed highly vibrationally excited, as is manifested by the broadness of the 1981 cm^{-1} band at early time delays and its long tailing toward lower wavenumbers. The small transient

(54) Two ν(CO) bands upshifted from their ground-state values are expected for LLCT/MLCT states, as calculated at 2026 and 2069 cm^{-1} by DFT/G03 in a vacuum for the $^3B_2$ state.

(55) Guillaumont, D.; Daniel, C. *Coord. Chem. Rev.* **1998**, *177*, 181−199.
(56) Goumans, T. P. M.; Ehlers, A. W.; van Hemert, M. C.; Rosa, A.; Baerends, E. J.; Lammertsma, K. *J. Am. Chem. Soc.* **2003**, *125*, 3558−3567.
(57) Pollak, C.; Rosa, A.; Baerends, E. J. *J. Am. Chem. Soc.* **1997**, *119*, 7324−7329.
(58) Baerends, E. J.; Rosa, A. *Coord. Chem. Rev.* **1998**, *177*, 97−125.
(59) Daniel, C. *Coord. Chem. Rev.* **2003**, *238−239*, 143−166.

feature at ~1935 cm^{-1} could correspond to the photoproduct excited in both the ν(CO) and low-frequency modes. The ca. 55 ps time constant of the formation of the *trans(I,I)*-[$Ru(I)_2(CO)(CH_3CN)(bpy)$] photoproduct corresponds to convoluted vibrational relaxation, final shift of the iodo ligands, and solvent coordination.

The presence of the IRuI-localized excited state state $^3A_2$ is manifested by the observation of the 1981 and 2045 cm^{-1} features at longer time delays. It is initially formed vibrationally excited in low-frequency modes. It cools with a time constant of 6−9 ps, as is documented by the upshift and narrowing of the 2030−2045 cm^{-1} absorption. The $^3A_2$ excited state is unreactive. Its ~155 ps decay matches the rate of the ground-state recovery.

The mechanism proposed above for *trans(I,I)*-[$Ru(I)_2(CO)_2$(bpy)] (Scheme 2) is in agreement with the rather low quantum yield (0.34) measured[31] for CO photosubstitution in *trans(I,I)*-[$Ru(I)_2(CO)_2$(4,4′-$(COOH)_2$-bpy)]. TRIR experiments show that the quantum yield is limited by the branching of the Franck−Condon LLCT/MLCT a^1A_1 excited-state evolution between CO dissociation and intersystem crossing to the unreactive ("trapping") IRuI-localized a^3A_2 state. The presence of a low-lying excited state in the iodo complex is further supported by the observation[31] of a low-energy (652 nm) emission from *trans(I,I)*-[$Ru(I)_2(CO)_2$(4,4′-$(COOH)_2$-bpy)] in low-temperature glasses.

The contrasting excited-state behavior of the chloro (and bromo) complexes as compared with the iodo complex can be understood in view of the singlet−triplet correlation diagram shown in Figure 4. The optically populated LLCT/MLCT b^1A_1 state of *trans(Cl,Cl)*-[$Ru(Cl)_2(CO)$(bpy)] can either react, decay to the ground state, or undergo intersystem crossing (ISC) to the a^3B_2 state of the same LLCT/MLCT origin. Decay to the ground state is expected to be slow because of a large energy gap. ISC to triplet states of a similar LLCT/MLCT character is slower than CO dissociation. On the other hand, *trans(I,I)*-[$Ru(I)_2(CO)_2$(bpy)] has two IRuI-localized triplet excited states a^3A_2 and a^3B_1 which lie at comparable or slightly lower energies than the b^1A_1 state. Intersystem crossing to these states is expected to be very fast because of different orbital origin with little involvement of the electronic system of the organic bpy ligand and a heavy-atom effect of both Ru and the I ligands. Fast ISC to these states provides an efficient relaxation pathway for the optically populated LLCT/MLCT b^1A_1 state, which competes with the ultrafast CO dissociation. The ^{3}IRuI-localized states are bound with respect to CO dissociation. Accordingly, analysis of changes in electron density distribution and calculated elongation of Ru−I bonds by 0.214 Å (Supporting Information) show that population of either a^3A_2 or a^3B_1 state weakens only the Ru−I bonds. The broadness and red-tailing of all the spectral features seen in the TRIR spectra of *trans(I,I)*-[$Ru(I)_2(CO)_2$(bpy)] at early time delays indicate that the inital vibrational excitation of the photointermediate, photoproduct, and triplet state is much more extensive than in the case of the chloro complex. This is probably caused by lower frequencies of all vibrations involving the heavy iodo ligands, which allow for excitation into higher vibrational levels.

Conclusions

The dynamics and mechanism of dissociation of an equatorial CO ligand from carbonyl−diimine complexes were unraveled using *trans(X,X)*-[$Ru(X)_2(CO)_2$(bpy)] (X = Cl, Br, I) as an example. For X = Cl and Br, optical excitation of the ^{1}LLCT/MLCT transition triggers femtosecond CO dissociation and X−Ru−X bending, that is followed by a 13−16 ps movement of an axial halide ligand to the vacant equatorial position. A *cis(X,X)*-[$Ru(X)_2(CO)(CH_3CN)$(bpy)] photoproduct is ultimately formed. For *trans(I,I)*-[$Ru(I)_2(CO)_2$(bpy)], the same reaction mechanism leads to a vibrationally hot photoproduct. Relaxed *cis(I,I)*-[$Ru(I)_2(CO)(CH_3CN)$(bpy)] is formed with a time constant of 55 ps. Importantly, the initial CO dissociation competes with intersystem crossing from the optically excited ^{1}LLCT/MLCT excited state into a IRuI-localized triplet excited state. This is an unreactive state, which decays directly to the ground state with a time constant of about 155 ps. The different excited-state behavior of *trans(Cl,Cl)*-[$Ru(Cl)_2(CO)_2$(bpy)] and *trans(I,I)*-[$Ru(I)_2(CO)_2$(bpy)] is explained by different energetic positions of IRuI-localized triplets relative to the ^{1}LLCT/MLCT states. The ^{3}ClRuCl-localized states are too high in energy to be populated for the chloro complex, but the ^{3}IRuI states lie much lower for the iodide. Their population by intersystem crossing from the ^{1}LLCT/MLCT states is possible energetically, while facilitated by the heavy-atom effect of the iodide ligands. The ^{3}IRuI-localized states act as "trapping states". Their population from the optically populated ^{1}LLCT/MLCT state is competitive with the femtosecond CO dissociation, limiting the photochemical quantum yield.

There is no fundamental difference in the rate and mechanism of photochemical dissociation of an equatorial and axial CO ligand from carbonyl−diimine complexes. They both occur with femtosecond rates on (nearly) dissociative excited-state potential energy surfaces. However, dissociation of an equatorial CO triggers a large restructuring of the coordination sphere, which takes place within a few tens of picoseconds.

Acknowledgment. EPSRC and COST Action D14 European collaboration program are thanked for their financial support.

Supporting Information Available: Table of calculated structures. This material is available free of charge via the Internet at http://pubs.acs.org.

IC049548N